NEW UPGRADING PROCESS FOR HEAVY OIL USING IRON/ACTIVE CARBON MIXTURE CATALYST

S.Terai, H.Fukuyama, S.Sawamoto, K.Ootsuka
Technology Research Center, Toyo Engineering Corporation
1818 Fujimi,Togo,Mobara,Chiba,297-0017,JAPAN

K.Fujimoto
Department of Applied Chemistry, School of Engineering
The University of Tokyo, Hongo, Bunkyo-ku, Tokyo,113-0033,JAPAN

Key words: hydrocracking, vacuum residue, pyrite/active carbon

Introduction

There are a lot of works and efforts on heavy oil upgrading process. Among them, hydrocracking process converts heavy oil into valuable distillable product minimizing coke formation by using catalyst which may be expensive in some cases and adopting very much high hydrogen pressure which may result in high cost. This paper introduces a mixture of pyrite and active carbon (AC) catalyst which may have advantages over supported metal type in catalyst preparation. The mixture catalyst enabled hydrocracking of vacuum residue (VR) under relatively low hydrogen pressure (7.0-10MPa). The effectiveness of the mixture catalyst on hydrocracking reaction was examined in relation to AC pore structure. The kinetics of reaction using lumping model was also studied to envisage the function of the mixture catalyst.

Experimental

Hydrocracking of VR of which properties are shown in Table 1 was carried out in a one-liter semi-batch magnetically stirred autoclave under constant hydrogen flow rate. Reaction conditions were as follows; VR charge 300g, hydrogen pressure 7.0-10MPa, reaction temperature 415-445°C.

Gaseous products were analyzed by gas chromatography and hydrogen sulfide by detecting tube. The content of naphtha (IBP-171°C), kerosene (171-232°C), gas oil (232-343°C), vacuum gas oil (VGO:343-525°C) and residue (Resid:525°C+) fraction in liquid product were determined by gas chromatography distillation method after separating catalysts and coke by filtration. The amount of coke was determined as toluene insoluble. The hydrocracking conversion was defined as follows; conversion [%] = (100-weight%525°C+ in products)/weight%525°C+ in feed VR.

Results and discussion

Effect of catalyst

The experimental results for various catalyst conditions listed in Table 2 are shown in Figure 1. The coke yield against conversion for each catalyst condition was observed to increase in the order Non-cat.≫Pyrite>Iron/AC≒Pyrite/AC mixture catalyst. In the case of non-catalyst, coke formation began at relatively early stage of conversion and significantly increased in successive reaction. Pyrite could suppress the coke formation only up to the range of 60% conversion. The combination of Iron and AC was examined in order to maximize distillable products with minimal coke formation. Iron supported on AC catalyst showed a good suppression ability of coke formation even through higher conversion level. The mixture of Pyrite and AC also showed the same ability to suppress coke formation as Iron supported on AC catalyst. The usage of mixture catalyst is thought to be advantageous in catalyst preparation

which does not necessitate impregnation with aqueous solution of metal salt, drying, and presulfidation.

Affinity of active carbon with VR

Adsorption tests were conducted to examine the affinity of AC with VR by immersing AC in VR under hydrogen pressure of 10MPa and temperature of 250°C at which cracking was expected not to occur. The quantity of adsorption on AC was defined as weight increase of AC after washing AC with toluene using Soxhlet extraction and vacuum drying. The degree of deasphaltene was calculated as reduction of asphaltene content remained in VR after adsorption. It was observed that AC had affinity with heavier fraction, especially asphaltene.

In order to investigate the relationship between AC pore structure and affinity with asphaltene, the adsorption tests in the same manner as above were carried out differing pore volume and mesopore ratio of AC in the order AC(C)>AC(A)>AC(B). As shown in Figure 2, AC(C) with well grown mesoporous structure exhibited the highest adsorption selectivity to asphaltene.

AC pore structure and Hydrocracking

The influence of AC pore structure on hydrocracking was studied. As shown in Figure 3, it was possible to attain higher conversion with less coke yield with AC which developed more mesoporous structure. From these experimental results, the hydrocracking in the presence of Iron/AC catalyst can be summarized as follows.

- Free radical intermediates are initially generated by thermal cracking of VR.
- Such intermediates are adsorbed on active carbon surface.
- Adsorbed intermediates are hydrogenated and stabilized by Iron and then desorbed from the active carbon surface.
- In the course of this reaction, AC with mesoporous structure provides free radical intermediates with proper sites for adsorption preventing them from polycondensing.

Kinetic study

Kinetic study was carried out to clarify the function and to quantitatively observe activity of catalysts for hydrocracking of VR. Reaction model using lumping species adopted here is illustrated in Figure 4. Residue fraction (525°C+) was classified into saturates (Satu), aromatics (Aroma), resins (Resin) and asphaltenes (Asp) by the method based on ASTM D4124-84 and products were grouped into Lo (Gas, Naphtha, Kerosene, Gas Oil),VGO and Coke. Each reaction path was fitted with experimental data by assuming first-order reaction. The comparison between calculated (lines) and experimental (keys) results for pyrite and pyrite/AC mixture are shown in Figure 5 (A) and (B), respectively. The agreement between calculated and experimental results are fairly good for both cases. The temperature dependence of reaction rate constants for pyrite and pyrite/AC mixture are shown in Figure 6 (A), and (B), respectively. Rate constants for cracking reaction to lighter products (Gas, Naphtha, Kerosene, Gas Oil) and condensation reaction (resins to asphaltenes) of pyrite catalyst were observed to be much sensible to temperature than those of pyrite/AC mixture catalyst. This suggests that pyrite catalyst tends to promote cracking reaction producing relatively lighter products on the one hand, and polycondensation producing asphaltene and finally coke on the other hand. However, pyrite/AC mixture catalyst proceeds reactions keeping middle fractions in products and restricting polycondensation of heavy components such paths from resins to asphaltene and asphaltene to coke. Thus the effectiveness of pyrite/AC mixture catalyst was also verified by this kinetic study.

Conclusions

The pyrite/AC mixture catalyst which is simple in preparation showed excellent effectiveness in hydrocracking of VR with the following results.

- AC with well grown mesoporous structure exhibited the highest adsorption selectivity to asphaltene.
- It was possible to attain higher conversion with less coke yield by using AC which developed more mesoporous structure.
- Kinetic study of reaction by lumping model also verified the effectiveness of pyrite/AC mixture catalyst.
- Hydrocracking was possible under relatively low hydrogen pressure by using mixture catalyst.

Thus pyrite/Active Carbon mixture catalyst was proved to be effective for upgrading of heavy oil with low hydrogen pressure condition.

Acknowledgments

This work has been carried out as a research project of the Petroleum Energy Center with the subsidy of the Ministry of International Trade and Industry, Japan.

Literature

Nakamura,I. and Fujimoto,K., PREPRINTS, Div. of Petro. Chem., ACS, 39(3),1994.

Table 1
Properties and Composition of Vacuum Residue

Feedstock			Middle East Blend VR
Density(15°C)		[g/cm3]	1.0334
Total Sulfur		[wt%]	4.02
Total Nitrogen		[wt%]	0.53
CCR		[wt%]	22.4
Metal	Ni	[wtppm]	53
	V	[wtppm]	180
C/H	C	[wt%]	84.8
	H	[wt%]	10.2

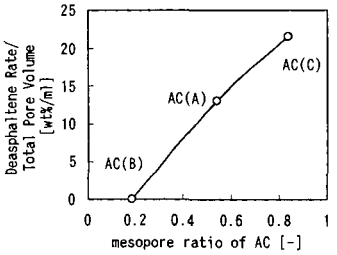

Figure 2 Mesoporous structure and adsorption selectivity of asphaltene

Table 2
Tested Catalysts

Case	Catalyst
1	Non Catalyst
2	Pyrite
3	Iron supported on AC Cat.(Iron/AC)
4	Pyrite/AC Mixture Cat.

AC:Active Carbon

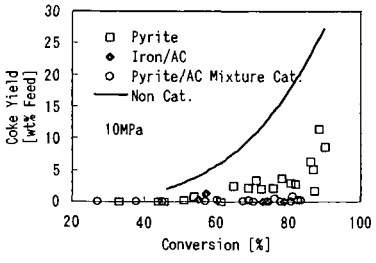

Figure 1 Hydrocracking results with several catalysts

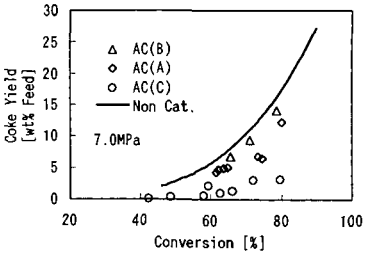

Figure 3 Relationship between porosity of AC and coke yield

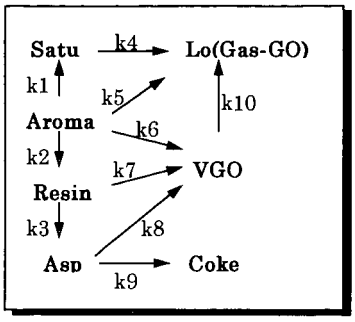

Figure 4 Reaction Model

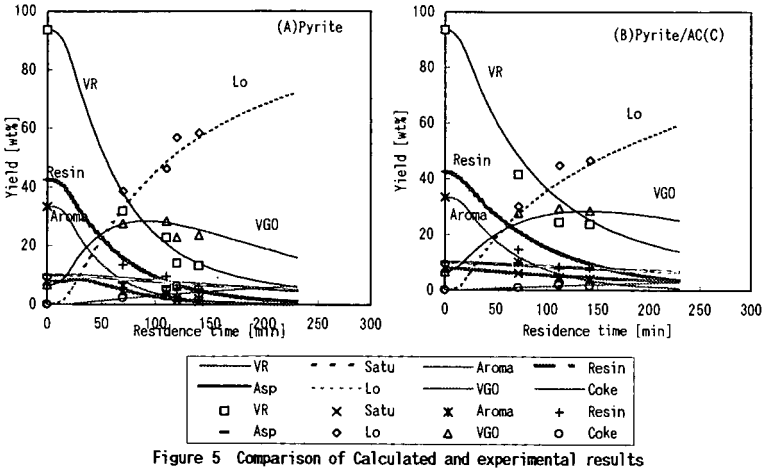

Figure 5 Comparison of Calculated and experimental results

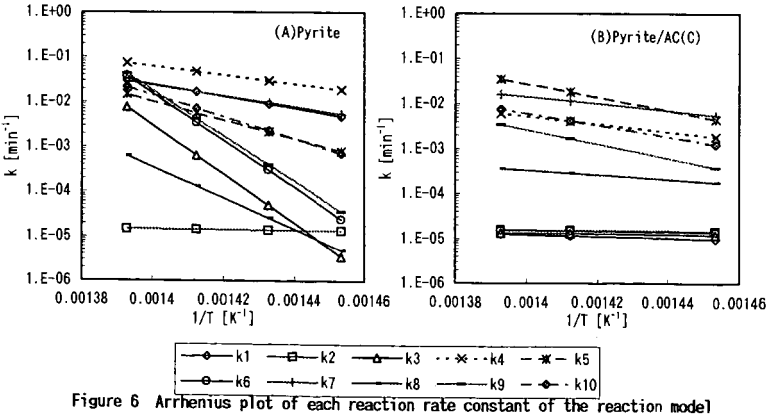

Figure 6 Arrhenius plot of each reaction rate constant of the reaction model

REMOVAL OF VOLATILE METAL CARBONYLS FROM RAW SYNGAS

R. Eijkhoudt, C.J. Smit*, A. J. van Dillen and J. W. Geus
Dept. of Inorganic Chemistry and Heterogeneous Catalysis, Utrecht University, Sorbonnelaan 16, 3584 CA Utrecht, The Netherlands. Email: R.Eijkhoudt@chem.uu.nl
* Shell Research and Technology Centre, Badhuisweg 3, 1031 CM Amsterdam, The Netherlands

Introduction

Industrial processes using carbon monoxide and/or hydrogen obtained from syngas can suffer from metal carbonyls originating from the feedstock used and the piping and reactor system. Nickel tetracarbonyl and iron pentacarbonyl, especially in combination with hydrogen sulfide, cause serious problems during the treatment of raw syngas and subsequent applications, mainly due to thermal and/or chemical carbonyl decomposition. For example, in gas treating processes using a liquid absorbent for the removal of acid gases, such as hydrogen sulfide and carbon dioxide in combination with a Claus plant, pressure build-ups, due to deposition of metal oxides/sulfides can be expected not only in the treating unit, but also throughout the Claus plant, especially on the catalyst bed of the first Claus reactor. In addition, downstream pressure-buildups may occur, as metal is being deposited on catalyst beds in syngas treating, e.g. COS hydrolysis and water gas shift. Furthermore, the active phase in the catalysts can become poisoned or show adversely changing activities and selectivity's due to the deposition of iron/nickel.

Generally, when CO is present in a gas stream as a reactant or (by) product in industrial processes, a suitable absorbent for nickel tetracarbonyl and iron pentacarbonyl often is imperative in order to eliminate or reduce the risk of catalyst poisoning, to extend plant operation life and to reduce the nickel and iron impurities in numerous chemical products originating from syngas.

In the research project described here, several high-surface oxides and zeolitic materials have been studied for their suitability to effectively remove metal carbonyls from raw syngas streams. The properties to be met with these materials are: applicable in a fixed bed, large capacity, regenerability and insensitivity for hydrogen sulfide and water.

Experimental

Absorbents

Several non-bindered zeolites and high-surface metal oxides have been studied for their ability to absorb iron and nickel carbonyls out of hydrogen sulfide and water containing syngas streams. High-surface SiO_2, Al_2O_3, Al_3PO_4, and zeolitic materials including ZSM-5 (MFI), mordenite (MOR), Y (FAU), Beta (BEA), UTD and MCM-41 were used in our experiments. In addition, different samples of faujasite were used, exhibiting a silica alumina ratio (SAR) ranging from 3 to 91. Faujasites with a SAR value higher than 3 had been de-aluminized by steam treating. All zeolitic materials exhibited a total pore volume of about 0.5 ml/g.

The samples were pelletized using a pressure of 1 MPa and subsequently crushed. A sieve fraction of 0.425-0.800 mm was used for absorption experiments. Prior to a measurement, the samples were treated in air for 24 hours at 523 K. Dehydration of the samples took place for 18 hours at 723 K.

Hexamethyldisiloxane (HMDS) was used to modify the hydrophilic character of the alumina and silica samples. This was established through boiling these materials in HMDS for one hour. In addition, the surface of alumina was treated with phosphoric acid in order to study the influence of the surface acidity. This was established through boiling this material in phosphoric acid for one hour.

Absorption experiments

Metal carbonyl absorption experiments were carried out in a fully automated microflow apparatus. In our experiments, simulated syngas was used, consisting of 40 vol.% H_2, 50 vol.% CO and 10 vol.% He. If required, water, hydrogen sulfide, metal carbonyl or a mixture of these components was added.

Prior to use, carbon monoxide was led at room temperature over a carbonyltrap consisting of zeolite Y. Water was introduced into the gas stream by means of a water saturator. Nickel tetracarbonyl was introduced into the gas stream by leading carbon monoxide over a reduced nickel catalyst (Ni/Al_2O_3, 70 wt.%) kept at 243 K. Iron pentacarbonyl was added to the feed by leading a controlled flow of helium through an iron pentacarbonyl saturator kept at 258 K. Helium 5.0, hydrogen 4.5, hydrogen sulfide 2.2 and carbon monoxide 4.7 were purchased from Hoek Loos b.v. Helium, hydrogen and hydrogen sulfide were used without further purification. The total gas flow was set at 100 ml/min, unless stated otherwise, so that an hourly linear space velocity was established of 6000 hr^{-1}. The iron pentacarbonyl and nickel tetracarbonyl partial pressures in the feed were varied between 0 and 30 Pa.

The gas composition upstream and downstream of the absorbent bed was analyzed with a Varian Cary 1E UV Vis spectrophotometer equipped with quartz gas flow cells with a length of 10 cm. The detection limit for iron pentacarbonyl was 0.01 Pa for iron pentacarbonyl, and for nickel tetracarbonyl 0.007 Pa. Furthermore, a Balzers quadrupole mass spectrometer was applied downstream of the bed for determination of the water and hydrogen sulfide partial pressures. 1 ml of absorbent sample (sieve fraction 0.425 to 0.800 mm) was placed in a quartz micro reactor tube (I.D. = 8 mm). If water and / or hydrogen sulfide were present in the gas stream, the absorbent bed was pre-saturated with water and/or hydrogen sulfide before the metal carbonyl was introduced in to the feed. Absorption profiles as a function of time were measured at 298 K. The total amount of metal carbonyl absorbed by the absorbent was calculated by integration of the metal carbonyl concentration difference up and downstream of the absorbent bed.

Absorbent Characterization

Pore size distributions and pore volumina were deduced from nitrogen absorption measurements with a Micromeretics 2000 gas absorption apparatus. The Horvath-Kawazoe model assuming a cylindrical pore geometry was applied.

Results and Discussion

To make a first selection, the suitability of a number of different absorbents was investigated. The influence of the chemical nature and the textural properties of the absorbent on the $Fe(CO)_5$ absorption capacity was examined using high-surface silica, high-surface alumina, zeolite Beta and Faujasite. All samples exhibited surface areas of 400 to 700 m^2/g. Syngas, only containing 20 Pa of iron carbonyl, was led over the absorbent bed. The results are summarized in Figure 1. From these results, it is clear that the zeolitic materials absorb significantly more metal carbonyl than the metal oxides. The absorption capacities of HMDS treated Al_2O_3 and SiO_2 are comparable with the absorption capacities of their unmodified counterparts. Also, the absorption capacity of untreated alumina is comparable with the absorption capacity of phosporic acid treated alumina.

The above findings led us to the conclusion that, when no additional compounds are present in the feed, the specific pore size and specific pore volume is far more important than the chemical nature of the surface for a suitable metal carbonyl absorbent.

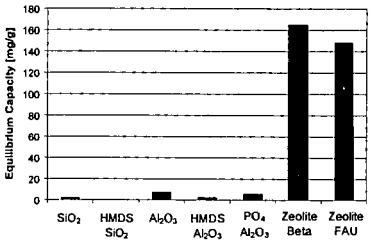

Figure 1: Equilibrium $Fe(CO)_5$ absorption capacities for several types of materials at 298 K. Hexamethyldisiloxane- treated SiO_2 and Al_2O_3 are denoted as HMDS-SiO_2 or HMDS-Al_2O_3, respectively. Al_2O_3 treated with phosphoric acid is denoted as PO_4-Al_2O_3.

Figure 2 displays the iron and nickel absorption capacity per gram of a number of zeolites as a function of pore size. Syngas, only containing 20 Pa of iron carbonyl or 16 Pa of nickel carbonylsulfide was led over the absorbent bed. From Figure 2 it becomes clear that zeolites exhibiting pores with a diameter less than 7 Å absorb only about 1 wt.% iron and nickel carbonyl. This suggests absorption to take place only at the external surface of these zeolite crystals. The kinetic diameter of the metal carbonyl molecules in the gas phase is about 7.4 Å, which is apparently too large to fit into the pore structure.

Zeolite Beta and Faujasite exhibit the largest absorption capacity. The pore (mouth) diameter of these materials is about the same size as the kinetic diameter of iron and nickel carbonyl. UTD and MCM, which have pores with a diameter larger than 8 Å, absorb significantly less. Their absorption capacity is found to be about one-third of the capacities for Beta and Faujasite. These results clearly reflect the

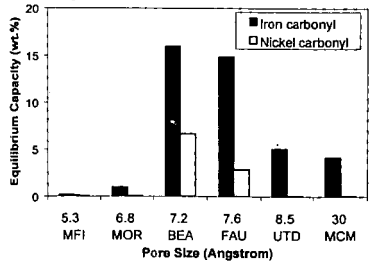

Figure 2: Equilibium absorption capacity at 298 K for Iron pentacarbonyl and Nickel tetracarbonyl as a function of the pore size. The zeolites used in this experiment are ZSM-5 (MFI), Mordenite (MOR), Faujasite (FAU), UTD, and mesoporous MCM-41

influence of the pore diameter on metal carbonyl absorption. For the zeolites tested, the capacity for nickel carbonyl is less than the capacity for iron carbonyl, although the kinetic diameters of iron and nickel carbonyl are about the same. It is beyond the scope of this abstract to go into detail on this issue. For the remainder of this abstract, we confine ourselves to faujasites and absorption of iron pentacarbonyl.

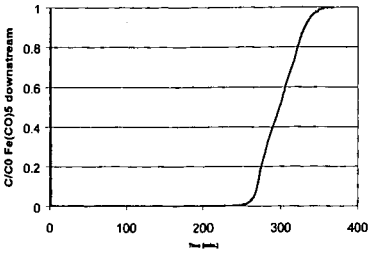

Figure 3: $Fe(CO)_5$ concentration downstream of an absorbent bed consisting of faujasite with a SAR value of 91.

A typical iron carbonyl absorption curve for a faujasite is displayed in Figure 3. Here, the carbonyl concentration downstream of the absorbent bed is plotted as a function of time. Syngas with 20 Pa of iron carbonyl was led over the absorbent bed. This breakthrough curve clearly shows that faujasites are capable of completely removing iron carbonyl out of a dry syngas stream.

Raw syngas contains also noticeable amounts of water and hydrogen sulfide. The question is, whether faujasites preferentially absorb water, hydrogen sulfide or metal carbonyl. Zeolite Y, a faujasite with a SAR value of 2.6, is known for its property to absorb water and, thus, it is used to dry gas streams. Therefore, it is imperative to study the influence of the SAR value on the absorption properties of faujasite for water, hydrogen sulfide and metal carbonyl separately, and in combination.

Syngas, containing both hydrogen sulfide (0.15 vol.%) and water (1.5 vol.%), but no metal carbonyls, was led over an absorbent bed consisting of faujasite with a SAR of 2.6 and 91, respectively. In Figure 4, both the H_2O and H_2S concentrations downstream of the absorbent bed are plotted as a function of time for both faujasites. For the faujasite with a SAR value of 2.6 it shows that initially both water and hydrogen sulfide are absorbed. However, as time progresses, hydrogen sulfide is desorbed from the zeolite and is expelled due to the absorption of water. A subsequently executed temperature-programmed desorption experiment showed only water to be present in the zeolite, the amount of which corresponds to complete pore filling. This result suggests that H_2O exhibits a considerably higher absorption energy than H_2S.
With the faujasite with a SAR value of 91, it turned out that only a small amount of water is absorbed, and no H_2S, since no desorption of H_2S due to absorption of water is measured.

A subsequent temperature-programmed desorption experiment showed that about 2 wt.% water is absorbed, and no hydrogen sulfide. These results demonstrate that from a gas stream containing both water and hydrogen sulfide, water is preferentially absorbed by faujasites.
The amount of water absorbed by the faujasite with a high SAR value, resembles a pore filling of only 4 percent. Therefore, we can conclude that only water might interfere with carbonyl absorption. Of course the extent of interference will be a function of the H_2O partial pressure.
De-aluminized faujasites are good candidates indeed for absorption of metal carbonyl from water and hydrogen sulfide containing gas streams. Additional absorption experiments showed no influence of hydrogen sulfide on the absorption kinetics of iron carbonyl.

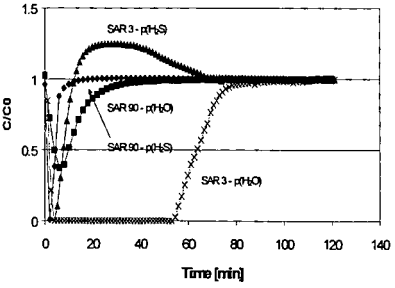

Figure 4: H_2O and H_2S concentrations downstream of the absorbent bed at 298 K, as a function of time onstream for two types of faujasites. The faujasites exhibit a silica alumina ratio of 2.6 and 91, respectively. C_0 is the concentration of H_2O and H_2S, respectively. $c(H_2O)$=1.5 vol.%, $c(H_2S)$=0.15 vol.%.

More information about the influence of water on the metal carbonyl absorption as a function of the SAR we obtained with the following experiments. Syngas, containing 20 Pa of iron carbonyl and either 0, 1.5 or 3 kPa of water, was led over the absorbent bed at 298 K. Figure 5 shows the equilibrium amount of absorbed iron carbonyl as a function of the SAR value, for a number of different H_2O partial pressures.

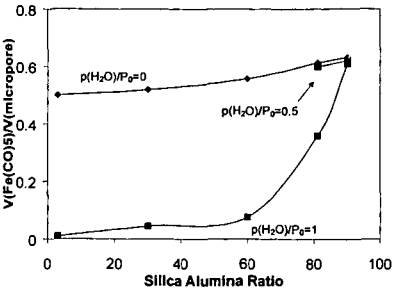

Figure 5: Volume $Fe(CO)_5$ absorbed in faujasite at 298 K, normalized on micro pore volume, as a function of silica alumina ratio and water partial pressure. For pore-filling calculations, it is assumed that $Fe(CO)_5$ absorbed in the micro pores has the same density as the bulk fluid.

From these results we can conclude that at relatively low SAR values, H_2O is preferentially absorbed in faujasites. Therefore, these faujasites exhibit little or no metal carbonyl capacity. However, at increasing SAR values, the influence of water on the amount of iron carbonyl absorbed decreases sharply. Typically, the equilibrium amount of $Fe(CO)_5$ absorbed by a faujasite with a SAR value of 91 is about 21 wt.%, regardless of the presence of water. The amount of water absorbed at $p(H_2O)/P_0=1$ for faujasites with SAR values of 3.6 and 91 is 31 wt.% and 17 wt.%, respectively. Apparently, at an increasing SAR value, the absorption energy of water in the micro pores decreases and metal carbonyl can get in. A high SAR value is therefore of major importance to effective metal carbonyl absorption. In other words, the SAR value is related to the hydrofobicity of the pores, and therefore of importance for lowering of the absorption energy of water. Also, a high SAR value appears to have a positive influence on the metal carbonyl absorption of the faujasites, probably due to textural changes by de-aluminization.

However, it can be expected that the presence of absorbed water for faujasites with a SAR value higher than about 60, obstructs the uptake rate of iron carbonyl to some extent. Lowering of the gas hourly space velocity (GHSV) could neutralize this effect. For the faujasite with a SAR value of 91, we assessed the influence of the GHSV on the iron carbonyl absorption kinetics in the presence of water.

Syngas, containing 3 kPa of water and 20 Pa of iron carbonyl, was led over the absorbent bed at 298 K. In Figure 6 the carbonyl concentration, downstream of the absorbent bed, is plotted as a function of the time for a GHSV of 6000/hr and 1500/hr, respectively. At a GHSV of 6000/hr, iron carbonyl was detected immediately. This was not the case for the dry faujasite at the same GHSV, as can be seen from Figure 3. After a steady state condition had been reached, the metal carbonyl concentration rose from 1.6 to about 2.2 Pa in 230 minutes. Finally, the concentration of metal carbonyl increased sharply, which indicated that the absorbent almost was saturated with iron carbonyl.

Lowering of the gas hourly space velocity from 6000/hr to 1500/hr, resulted in complete removal of iron carbonyl from the gas stream, as is usual for the dry faujasite at a GHSV value of 6000/hr. For both space velocities, the uptake of iron carbonyl remains 21 wt.%, corresponding with a micro pore filling of 65%. The uptake of water remains 17 wt.%.

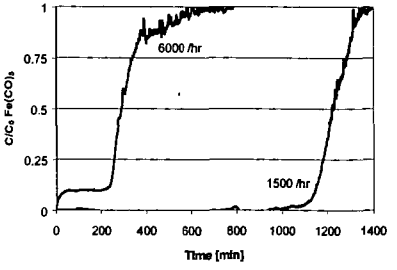

Figure 6: $Fe(CO)_5$ breakthrough curves at 298 K for a faujasite with a SAR value of 91, previously saturated with water. The gas hourly space velocity is varied between 6000 and 1500 /hr.

The results above led us to the conclusion that lowering of the GHSV neutralizes the retarding effect of water on the uptake rate of iron carbonyl. This retarding effect of water can only be explained by assuming that either water is rather easily expelled from the micro pore system of the faujasite due to absorption of iron carbonyl, or water is preferentially absorbed outside the micro pores. The exact nature of the influence of water on carbonyl absorption by de-aluminized faujasites goes beyond the scope of this abstract and will not be discussed here.

Finally, for application in an industrial process, these materials need to be regenerable. Bath [1] and Golden [2] already showed for zeolite Y that gentle heating restores completely the initial absorption capacity. Eijkhoudt et al. [3] showed the same for de-aluminized faujasites.

Conclusions

When carbon monoxide is present in a gas stream as a reactant or (by) product in industrial processes, a suitable absorbent for nickel tetracarbonyl and iron pentacarbonyl often is imperative. Faujasites with a silica alumina ratio of 60 and higher prove to be excellent metal carbonyl absorbents with regenerable capacities up to 21 wt.%, which corresponds to a micro pore filling of 65 %. Under the conditions applied, our experiments show that the metal carbonyl absorption capacity of these faujasites is influenced neither by hydrogen sulfide nor water. However, water retards the uptake rate of metal carbonyl to some extent. This retarding effect is easily neutralized by lowering of the gas hourly space velocity.
Consequently, these absorbents can be used to remove volatile metal carbonyls from raw syngas streams.

Acknowledgements
Shell Research and Technology Centre b.v. for financial support of this research.
Dr. Bonnie Marcus from Zeolyst International, for providing zeolite samples.
Dr. P.J. van den Brink and Dr. E.J. Creyghton from SRTCA Amsterdam for providing samples and for helpful discussions.

1 B. L. Bhatt, *Sep. Sci. and Techn.* 26 (1991), 1559.
2 T.C. Golden, *Ind. Eng. Chem. Res.*, 30 (1991), 502.
3 R. Eijkhoudt, "*Formation and Removal of volatile Metal carbonyls*", thesis, to be published.

SULFUR-RESISTANT BIMETALLIC NOBLE METAL CATALYSTS FOR AROMATIC HYDROGENATION OF DIESEL FUEL

Linjie Hu*, Hong Nie, Lianglong Qu, Guofu Xia, Yahua Shi, Dadong Li

Research Institute of Petroleum Processing, SINOPEC, Beijing 100083, PRC
Phone Number: 010-62315897 X 3862

INTRODUCTION

It is recognized that high aromatic content will lower the cetane number of diesel fuel and contribute significantly to the formation of undesired emissions in exhaust gases. As a result of the stringent environmental regulations, lowering aromatic content in diesel fuel is one of important technologies. Aromatic hydrogenation, especially for monoaromatics, is more difficult than hydrodesulfurization (HDS) and hydrodenitrogenation (HDN) on conventional sulfide catalysts (1). In addition to this, there is thermodynamic equilibrium limitation on aromatic hydrogenation within the normal operating range of hydrorefining. Therefore, the deep hydrodearomatization (HDA) is a formidable task by conventional hydrotreating technology using supported Ni(Co)Mo(W) sulfide catalysts.

Two-stage hydrotreating routes have been recommended to achieve low level of aromatics for its less investment in facilities and lower operating costs (2-5). In a two-stage process, a sulfide catalyst is used in the first stage where the sulfur and nitrogen are brought down, and a sulfur-tolerant noble metal catalyst is used in the second stage for aromatic hydrogenation. The key of the two-stage process is the development of high active noble metal catalyst with fine sulfur-resistance.

It has been generally acknowledged that the sulfur resistance of a noble metal can be enhanced by utilizing an acidic support, such as that of an acidic zeolite (6-14). Literatures on the sulfur resistance of bimetallic catalysts containing noble metals, except for Pt-Pd, are scarce (15). Y-zeolite supported noble metal catalysts, as important industrial catalysts for aromatics hydrogenation, have received increasing attention in recent years (16). Pd-M/Y bimetallic catalysts, where M are non-noble metal elements, were prepared to investigate the effects of the addition of a second metal in this study.

EXPERIMENTAL

70g NH_4Y (Na 1.2%, SiO_2/Al_2O_3=5) was mixed with 30g Al_2O_3, followed by kneading and extrudation, and finally calcined at 600°C for 2h.

The catalyst samples were prepared by incipient wetness impregnation technique. The Y zeolite support was brought in contact with a solution of $Pd(NH_3)_4Cl_2$ in deionized water, followed by drying at 120 for 2h and then calcining at 550 °C for 2h.The palladium-contained Y zeolite contacted with an aqueous solution of $(NH_4)_2CrO_4$, then dried and calcined as before. The Pd-Cr/Y catalyst has been prepared.

The other Pd-M/Y bimetallic catalysts were prepared following the same procedure with Pd-Cr/Y. The second metal precursors used for the preparation of the bimetallic catalysts are listed in Table 1. The metal contents, which were measured by inductively coupled plasma spectroscopy, are also listed in Table 1.

The sulfur resistance of catalyst was tested with a continuous down flow fixed-bed reactor. The reactor was packed with 1.0g catalyst (40~60 mesh) diluted with an inert 40~60 mesh ceramic in a ratio of 1:1. The upper and bottom part was filled with particles of a catalytically inactive ceramic material for preheating and preventing channel effects. The feed, toluene and n-hexane in a volume ratio of 1:1, was mixed with a certain amount of thiophene to prepare a feed of 3000ppm sulfur content. Catalysts were firstly reduced at 300 °C under 600psig of pure hydrogen for 2h. After reduction, the catalytic reactions were carried out with a weight hourly space velosity (WHSV) of $4.0h^{-1}$ and flowing hydrogen (400ml/min), under 600psig. Reaction products were analyzed by an on-line gas chromatography.

RESULTS AND DISCUSSION

The GC analysis results indicate that the main products of toluene hydrogenation on Pd-M/Y catalysts are methylcyclohexane(MCH) and 1,1-dimethyl cycloheptane (DMCH).

Fig.1 and Fig.2 show that hydrogenation activity of Pd-M/Y bimetallic catalysts are remarkably

different from Pd/Y catalyst, though the second metal added was only 0.6%. This indicates that the sulfur resistance of Pd are remarkably affected by the second metal. The sulfur resistance of Y zeolite supported Pd catalyst is improved by Cr and W, but lowered by La, Mn, Mo, Ag.

Fig.3 indicates that the second metal have no effect on the product selectivity of toluene hydrogenation on Pd bimetallic catalysts. The formation of isomer DMCH is related to the acidic properties of catalysts. The isomer selectivity doesn't change with the addition of the second metal. It could be deduced that the second metals have no effects on the acidic properties of Pd catalysts.

It can be observed from Fig.1 and Fig.2 that PdCr/Y and PdW/Y bimetallic catalysts exhibit better sulfur resistance than Pd/Y. This phenomena has not found to be reported yet. Since Y zeolite supported noble metal catalysts is important on industrial aspects, this discovery would have applied prospects for petroleum processing. From the aspects of isomer selectivity of toluene hydrogenation on Pd monometallic and bimetallic catalysts, the change of sulfur resistance of Pd catalysts was not caused by acidic properties. Nowadays, further studies on the mechanism that the second metal affects the sulfur resistance of Pd catalysts are carrying on in our laboratory.

CONCLUSIONS

The second metal has remarkable effects on the sulfur resistance of Y zeolite supported Pd catalysts. Among them, Cr and W improve the sulfur tolerance of Pd catalysts, but La, Mn, Mo and Ag make the sulfur resistance worse. For catalytic hydrogenation of toluene in presence of 3000ppm sulfur in feed on Pd/Y and Pd-M/Y, the second metals(M) have no obvious effects on product selectivity.

ACKNOWLEDGEMENTS

The support of Xiaohong Kang and Group 1508, Research Institute of Petroleum Processing are acknowledged.

Table 1. Summary of Catalyst Preparation and Composition

Catalyst	Precursor of Second metal	Pd content (wt%)	Second metal (wt%)
Pd	-	0.61	0
PdCr	$(NH_4)_2CrO_4$	0.59	0.61
PdW	$(NH_4)_{10}W_{12}O_{41}\cdot 11H_2O$	0.59	0.59
PdLa	$La(NO_3)_3$	0.60	0.60
PdMn	$Mn(NO_3)_2$	0.60	0.60
PdMo	$(NH_4)_2MoO_4$	0.60	0.59
PdAg	$AgNO_3$	0.61	0.61

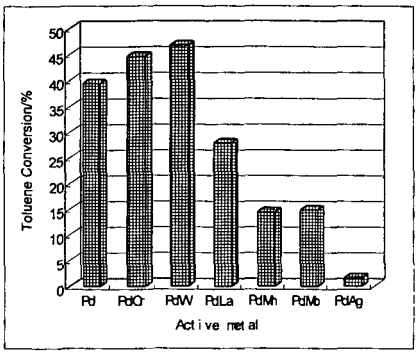

Fig.1 Toluene conversion on Pd bimetallic catalysts(T=280)

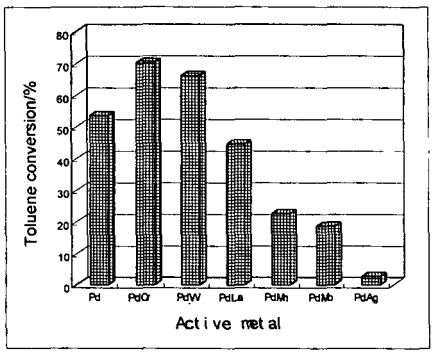

Fig.2 Toluene conversion on Pd bimetallic catalysts(T=300)

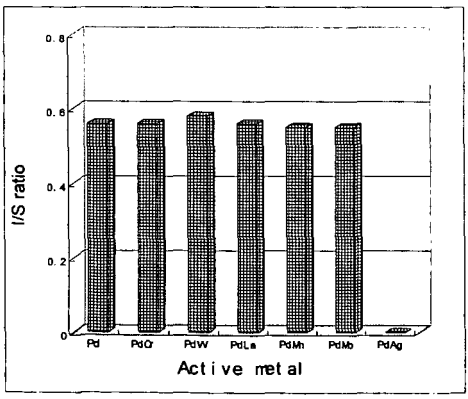

Fig.3 Isomerization selectivity(I/S ratio)
on Pd bimetallic catalysts
T=280°C

LITERATURE CITED

(1) Cooper, B. H., Stanislaus, A. and Nannerup, P. N., Am. Chem. Soc. Div. of Feul Chem. Preprints, 37(1), 41 (1992)
(2) Suchanek, A. J., Karlsson, K., 1993 NPRA Annual Meeting, AM-93-24
(3) Baldassari, M. C., 1994 NPRA Annual Meeting, AM-94-62
(4) Suchanek, A. J., Hamilton, G. L., 1992 NPRA Annual Meeting, AM-92-19
(5) Suchanek, A. J., Hamilton, G. L., 1991 NPRA Annual Meeting, AM-91-35
(6) Gallezot, P., Bergeret, G., Catalyst Deactivation, Dekker, New York, p.263(1987)
(7) Suchanek, A. J., Oil Gas J, May 7, p.109(1990)
(8) Peries, J. P., Billon, A., Hennico, A., Kressmann, S., 1991 NPRA Annual Meeting,
(9) Dalla Betta, R. A., Boudart, M., Proc. 5th Int. Congr. on Catal., North Holland, p.1329(1973)
(10) Homeyer, S. T., Sachtler, W. M. H., Zeolites: Facts, Figures and Future, Elsevier, p.975(1989)
(11) Rabo, J. A., Schomaker, V., Pickert, P. E., Proc. 3rd Int. Congr. on Catal., North Holland, Amsterdam, p.1264(1964)
(12) Chukin, C. D., Proc. 6th Int. Congr. Catal., Chemical Society, London, p.668(1977)
(13) Tri, T. M., Massardier, J., Gallezot, P., Imelik, B., Stud. Surf. Sci. Catal., 5, 279(1980)
(14) Besoukhanova, C., Stud. Surf. Sci. Catal., 6, 201(1980)
(15) Cooper, B. H., Donnis, B. B. L., Appl Catal A: General, 137, 203(1996)
(16) Stanislaus, A., Cooper, B. H., Catal. Rev. Sci. Eng., 36, 75(1994)

OPTIMUM DESIGN OF THE NICKEL CATALYSTS AND MECHANISTIC STUDY FOR CO_2 REFORMING WITH CH_4

Rong-Gang DING Zi-Feng YAN *
State Key Laboratory for Heavy Oil Processing, University of Petroleum, Dongying 257062, P R China

ABSTRACT The possibility of optimizing the composition and the structures of the nickel catalysts and the pretreatment and reaction conditions for carbon dioxide reforming with methane is investigated. The optimum catalyst and the pretreatment and reaction conditions are determined employing the orthogonal and uniform design methods. The optimum nickel catalyst gives promising catalytic performance in terms of activity, selectivity and resistance to coke formation under the pretreatment and reaction conditions. The reaction behaviors and perfect performance of the optimum catalyst are extensively discussed. The properties of the surface carbon intermediates, which are produced by the decomposition of methane, using temperature-programmed desorption, temperature-programmed surface reaction, pulse reaction and on-line quadrupole mass spectroscopy techniques were also investigated. Carbidic C_α, carbonaceous C_β and carbidic clusters C_γ surface carbon species formed by decomposition of methane showed different surface mobility, thermal stability and reactivity. The possible reaction mechanism of carbon dioxide reforming with methane will also be postulated. Methane is firstly decomposed into hydrogen and different surface carbon species, then the adsorbed or gas phase CO_2 reacts with surface carbons to form CO.

KEYWORDS Optimum design, carbon dioxide reforming with methane, mechanism

1. INTRODUCTION

In recent years, catalytic reforming of carbon dioxide with methane to synthesis gas has been received new interest due to its environmental benefits and desired CO/H_2 ratio than steam reforming for the production of hydrocarbons and oxygenated derivatives. Unfortunately, no commercial catalyst is yet available for the reforming of methane with carbon dioxide. Supported noble metals give promising catalytic performance in terms of activity, selectivity and resistance to coke formation.[1-3] Various nickel-based catalysts have been prepared and investigated in the past decades[4-6] with different metal loadings, varieties and quantities of the promoters, and kinds of the supports. But there are few reports comparing the activity and stability of the catalysts with different compositions. No effective method to arrange the catalyst preparation and activity evaluation has yet been proposed. This paper aims at exploring possibility of optimizing the composition of the nickel catalysts and the pretreatment and reaction conditions employing orthogonal design and uniform design methods. There is a limiting amount of fundamental research concerning the reforming of methane with carbon dioxide over nickel-based catalysts. The present study also reports the characterization of the surface carbon intermediates produced in the reforming process and postulation of the reaction mechanism.

2. EXPERIMENTAL

2.1 Catalyst Preparation. A series of nickel-based catalysts were prepared with different supports, promoters and metal contents. La_2O_3, SiO_2, and two kinds of Al_2O_3 are selected as the catalyst supports. Nickel nitrate was loaded on the various supports by the incipient wetness impregnation method, then magnesium nitrate and cerous nitrate were added to the support by the same method. The nickel loading was set from 7.0% to 11.5% (wt%), while each promoter content was kept from 0 to 3% (wt%).

2.2 Catalytic Reaction. The reforming reaction was carried out in a continuous flow quartz fixed-bed reactor (i.d. 6mm) under atmospheric pressure and various reaction temperatures. The composition of reactants/products mixture was analyzed with an on-line SP-3420 gas chromatograph equipped with a TCD and a Porapak QS column.

2.3 Catalyst Characterization. The temperature-programmed experiments are conducted in the quartz fixed-bed reactor following the catalysts pretreatment. The catalysts are treated with oxygen for 30 min, then reduced with H_2 for 1 hr, finally cooled to room temperature and purged with He stream for 30 min.

* To whom correspondence should be addressed. E-mail: zfyan@hdpu.edu.cn

The methane was pulsed continually on the pretreated catalysts using high purity helium as carrier gas at 973 K. Subsequently, a 20 ml/min flow of hydrogen or mixed gas of CO_2/He (1:10) was introduced to flush the reactor continuously to take away the gaseous and physically adsorbed mixture after cooling to room temperature. Then the TPSR was initiated in the hydrogen or mixed gas of CO_2/He at a heating rate of 20 K/min. When the temperature was

increased to 1000 K, the carrier gas was switched again, then H_2 and O_2 were pulsed respectively into the micro-reactor under high temperature. The desorbed products from the metal surface along with the temperature-programmed process were simultaneously detected by on-line ion trap detector (ITD).

TPD experiments were conducted at a constant heating rate (10 K/min), using ultra high purity helium as carrier gas, at a flow rate of 40 ml/min. The reforming reaction was carried out in situ at certain temperature and then the reactor was quickly cooled to room temperature. After purging with He for 30 min, the temperature programming was initiated and the analysis of the desorbed gases was performed with the on-line ITD.

In the TPD process, the helium gas was dried with $Mg(ClO_4)_2$ and deoxygenated with 402 deoxygenating reagent. The residual oxygen that might flow over the catalyst was removed by using liquid nitrogen cold trap before flowing into the reactor. Leak tests on the reaction system were also strictly performed to exclude the possibility of the oxidation of surface carbonaceous species.

3. RESULTS AND DISCUSSION

3.1 Catalyst Optimization. A series of nickel-based catalysts, with various supports, promoters and metal loadings, were prepared by incipient wetness impregnation method according to a certain orthogonal design table. The L_{25} (4^5) orthogonal table is employed to arrange the preparation of catalysts and investigate the interaction between metal and support. In this table, the support-metal strong interaction was considered an important factor. The orthogonal design experimental results for the reforming catalyst are shown as Table 1.

The optimum pretreatment and reaction conditions were determined by a large number of experiments employing the uniform method. Its characteristic and application in the catalytic scientific community will be discussed elsewhere. Catalytic performance tests for all catalysts were carried out under the optimum pretreatment and reaction conditions.

The total molar concentration of CO and H_2 (dry base) is used to evaluate the performance of catalysts. It can be seen that the effect of the factors on the performance of the catalyst is as follows: support > Ni metal loading > MgO addition > CeO_2 addition > interaction between metal and support. It is found that the support shows more influence than metal loading on the performance of catalysts within appropriate metal loading range. It gives evidence that understanding of the nature of support and selection of support may be very important for improving the catalyst.

The weak interaction between metal and support may be attributed to the preparation conditions of the catalysts. In the meantime, MgO and CeO_2 promoter exhibit approximate effect on the activity of catalysts. It can be seen from Table 1 that the OD-5 catalyst is the best reforming catalyst in this experiment. Indeed, it provides 91.3% and 86.9% conversions of CO_2 and CH_4, 86.8% and 89.1% yields of H_2 and CO at 973K, respectively. According to the experimental results, it is deduced that the optimum catalyst constitutes can be described as follows: 8.5 wt% Ni loading supported on Al_2O_3-1 with 3 wt% MgO and 3 wt % CeO_2 added.

The catalyst activity exhibited in Table 1 is the integrative result of the collective effect of metal loading, support, promoter, and interaction between support and metal. It is very difficult to simply compare one catalyst with another in terms of certain factor's influence on the performance of catalyst when the catalyst are prepared and tested according to a orthogonal design method. The orthogonal design considers all factors as an indivisible one and arranges them efficiently to simplify the catalyst screening. For the heavy and complicated catalyst screening, the orthogonal design method may be a desired choice. As a matter of fact, the orthogonal design method has applied to many scientific fields. But to our knowledge less applications of the orthogonal design in catalyst preparation and screening have been reported. In this work, we try to make use of this method to optimize the catalyst and simplify the catalyst screening process. It is convinced of the rapid development of the catalyst orthogonal screening technique in near future.

3.2 Catalyst Characterization.

H_2 TPSR of the catalyst. A great effort was made to detect adsorbed carbonaceous $CH_{x(ad)}$ fragments formed in the decomposition of methane by means of sensitive *in-situ* FT-IR spectroscopy. However, no adsorption bands attributable to any vibration modes of carbonaceous $CH_{x(ad)}$ species were identified either by *in-situ* measurements or after a sudden cooling of the sample in a continuous methane flow at 700 K. This means that all the above carbonaceous $CH_{x(ad)}$ species react or decompose too quickly at high temperature, or their surface concentrations are below the detection limit.

However, the presence of surface carbonaceous $CH_{x(ad)}$ species was well manifested by its reaction with hydrogen. After flushing the reactor with pure helium flow (following methane decomposition at a certain temperature) and switching to a hydrogen flow, the hydrogenation of the surface carbonaceous $CH_{x(ad)}$ species was investigated by TPSR technique. Figure 1 showed that the decomposition of methane could result in the formation of at least three kinds of surface

carbon species on supported nickel catalyst. Generally, the carbon deposition is comprised of various forms of carbon species which are different in terms of reactivity. The distribution and features of these carbonaceous species depend sensitively on the nature of transition metals and the conditions of methane adsorption. These carbonaceous species can be described as: completely dehydrogenated carbidic C_α type, partially dehydrogenated CH_x ($1 \le x \le 3$) species, namely C_β type, and carbidic clusters C_γ type formed by the agglomeration and conversion of C_α and C_β species under certain conditions.

A fraction of the surface carbon species, which might be assigned to carbidic C_α (~461 K), was mainly hydrogenated to methane even below 500 K. Simultaneously, a trace of ethane was also produced in addition to methane. It shows that carbidic C_α species is rather active and thermally unstable on nickel surface. The significant amount of surface carbon species was hydrogenated to methane below 600 K and was assigned to partially dehydrogenated C_β (~583 K) species. The majority of the surface carbon was hydrogenated above 800 K and was attributed to carbidic clusters C_γ (~823 K). The formation of less active C_γ species causes the catalyst deactivation.[8] It also indicated that the formation of three kinds of surface carbon species with different structures and properties largely depend on the exposure temperature and duration to methane. When the nickel catalyst was exposed to methane above 723 K, the carbidic C_α species was not detected, and a significant amount of C_β was transformed into the carbidic clusters C_γ. It shows that the carbidic clusters C_γ species might be the precursor of the surface carbon deposition, which may be produced by the interactions between C_α and C_β species and between C_α and C_β themselves.

TPD of used catalyst. The TPD profiles of used Ni/Al_2O_3 catalyst after 8 h of reaction were shown in Figure 2. Compared with CO-TPD profiles over the fresh Ni/Al_2O_3 catalyst, on which two respective CO_2 desorption peaks appear, an additional intense CO_2 peak at ca. 910 K was observed on used catalyst.

The two CO_2 desorption peaks appear on both the TPD of used catalyst and the CO-TPD profiles over the fresh catalyst at ca. 410 K and 570 K. They seem to correspond to the desorbed CO_2 in the form of weakly chemisorbed on different sites on both catalysts. It is interesting to note that a large quantity of CO and CO_2 desorbed at approximately the same temperature from at ca. 800 K, but the increase of CO obviously lagged behind. This indicates that CO might be the secondary product rather than primary one. The interaction of surface carbon with gaseous CO_2 would result in the formation of CO. The obvious hysteresis effect of CO peak with respect to CO_2 peak and the continuous increase of intensity of CO peak are noteworthy. This could be manifested by the mobility of the surface carbon species and the reactivity of the oxygen species on the nickel catalyst. The mobile surface carbon species can attack the neighboring oxygen adatoms and surface oxygen species to form CO or CO_2. It is also possible that the CO_2 desorbed from the catalyst re-adsorbed and then reacted with surface carbonaceous species to produce CO. The carbon species originally produced by methane are believed to be atomic or carbidic carbon. It is known to be a very active and important intermediate in the CO_2 reforming of methane. The interaction between the adsorbed or gaseous CO_2 and surface carbon species can result in the formation of CO. Based on this consideration, the possible reaction processes of CO_2 reforming of methane can be inferred as follows: methane is firstly decomposed into hydrogen and different surface carbon species, then the adsorbed or gas phase CO_2 reacts with surface carbons to form CO.

CO_2 TPSR and pulse reaction of H_2 and O_2. Firstly, TPSR was performed in the mixed gas of CO_2/He (1:10) following CH_4 pulses over reduced Ni/Al_2O_3 catalyst (Figure 3), then the H_2 or O_2 pulse was introduced into the reactor (Figure 4). A fraction of CO_2 adsorbs on the catalyst at about 300 K and desorbs from 600 K in the CO_2/He flow. The equilibrium between the surfaced adsorbed and gaseous CO_2 is responsible for the high CO_2 desorption temperature than that in He flow. The formation and desorption of CO can be observed while surfaced CO_2 begins to desorb greatly. The consumption of CO_2 and formation of CO reach the maximum at elevated temperature of 740 K. The CO_2 TPSR on the Ni catalyst may give a deduction of the pathway of CO_2: firstly adsorbs on the surface of the catalyst, then reacted with neighboring surface carbonaceous species to form CO. This is similar to the inference from the TPD experiment of the used catalyst as Figure 2 showed.

The formation of CH_4 is not detected in the H_2 pulse reaction following CO_2 TPSR at 973 K. It shows that the surface carbonaceous species which can react with CO_2 have used up. This type of surface carbonaceous species is active and can react with not only CO_2 but also with H_2. At the same time, other inertial carbonaceous species may exist on the surface of the catalyst. The O_2 pulse reaction is continually carried out following the CO_2 TPSR and H_2 pulse reaction in order to verify the existence of other carbonaceous species. The appearance of CO_2 corresponding to the O_2 pulses is good evidence for the existence of the other carbonaceous species, which is difficult to react with H_2 or CO_2. The catalyst deactivation may result from the deposited carbon species, which does not react with H_2 or CO_2 but react with O_2 at high temperature.

Figure 1 becomes conscious of the emergence of at least three kinds surface carbonaceous species at lower temperature. When the catalyst was exposed to methane at 973 K, the carbidic C_α species was completely converted into C_β or C_γ species. The partially dehydrogenated C_β

species can react with H_2 or CO_2 to form CH_4 or CO, but the less active carbidic clusters C_γ species can not react with H_2 or CO_2 even at very high temperature. The H_2 and CO_2 TPSR and pulse reaction provide the mutual verification of the existence and property of the surface carbonaceous species. The further investigation towards the properties of the surface carbon species is the key to suppressing the catalyst deactivation and elucidating the mechanism of the reforming reaction.

4. CONCLUSIONS

(1) The orthogonal design method can simplify the catalyst screening process and evaluate the principal effect and its degree of influence on the performance of the catalyst.
(2) Carbidic C_α, carbonaceous C_β and carbidic clusters C_γ surface carbon species formed by decomposition of methane showed different surface mobility, thermal stability and reactivity. C_α and C_β species are active and the carbidic clusters C_γ species might be the precursor of the surface carbon deposition.
(3) The possible reaction processes may be as follows: methane is firstly decomposed into hydrogen and different surface carbon species, then the adsorbed or gas phase CO_2 reacts with surface carbons to form CO.

ACKNOWLEDGEMENTS

Financial supports by the Young Scientists Award Foundation of Shandong Province and Young Scientists Innovation Foundation of China National Petroleum Corporation are gratefully acknowledged.

REFERENCES

(1) Solymosi, F.; Kustan, G.; Erdohelyi, A. *Catal. Lett.* **1991**, *11*, 144.
(2) Vennon, P. D. F.; Green, H. M. *Catal. Today* **1992**, *13*, 417.
(3) Richardson, J.T.; Paripatyadar, S.A. *Appl.Catal.* **1990**, *61*, 293.
(4) Gadalla, A.M.; Bower, B. *Chem. Eng. Sci.* **1988**, *43*, 3049.
(5) Yamazaki, O.; Nozaki, T.; Omata, K.; Fujimoto, K. *Chem. Lett.* **1992**, 1953.
(6) Chen, Y. G.; Yamazaki, O.; Tomishige K.; Fujimoto, K. *Catal. Lett.* **1996**, *39*, 92.
(7) Wang, S. B.; Lu, G. Q. *Ind. Eng. Chem. Res.* **1997**, *36*, 5103.
(8) Zhang, Z.; Verykois, X. E. *Catal. Today* **1994**, *21*, 589.

Table 1 Orthogonal design experimental results
(T = 973 K, P = 1atm, CH_4 / CO_2 = 1.05)

factor	A	B	A	B	C	D	$(CO+H_2)$	CH_4	CO_2	H_2	CO
	Ni		MgO		CeO_2		concn.(dry	conv.	Conv.	yield	yield
number	(wt%)	support	(wt%)		(wt%)		mol%)	(%)	(%)	(%)	(%)
1	7.0	Al_2O_3-1	1	0	0		71.2	74.6	79.7	74.0	77.2
2	7.0	Al_2O_3-2	2	1	1		75.8	79.5	85.7	784	82.6
3	7.0	La_2O_3	3	2	2		46.5	48.7	54.6	47.0	51.7
4	7.0	SiO_2	4	3	3		68.1	69.7	77.0	67.9	73.4
5	8.5	Al_2O_3-1	2	2	3		84.8	86.9	91.3	86.8	89.1
6	8.5	Al_2O_3-2	1	3	2		79.2	81.9	89.3	80.3	856
7	8.5	La_2O_3	4	0	1		54.3	57.7	68.7	53.8	63.2
8	8.5	SiO_2	3	1	0		61.4	64.3	71.5	62.4	67.9
9	10	Al_2O_3-1	3	3	1		77.3	79.9	86.8	78.5	83.4
10	10	Al_2O_3-2	4	2	0		66.5	68.7	75.1	67.3	71.9
11	10	La_2O_3	1	1	3		52.4	54.0	61.1	51.9	57.8
12	10	SiO_2	2	0	2		56.3	58.4	61.6	58.3	60.0
13	11.5	Al_2O_3-1	4	1	2		62.3	64.6	73.4	62.0	69.0
14	11.5	Al_2O_3-2	3	0	3		59.3	62.0	69.1	60.0	65.6
15	11.5	La_2O_3	2	3	0		48.9	51.2	59.2	48.6	55.3
16	11.5	SiO_2	1	2	1		49.6	51.6	59.3	49.2	55.5
R			14.9	23.4	3.7	8.1	7.1				
prior level			A_2	B_1	$(A\ B)_2$	C_4	D_4				
factor order			2	1	5	3	4				

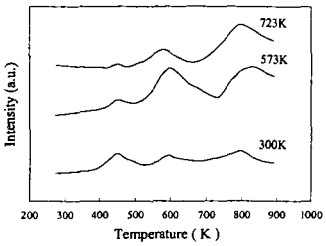

Figure 1. TPSR spectra of CH_4 in H_2 flow on fresh 8wt% Ni/Al_2O_3 at different adsorption temperatures

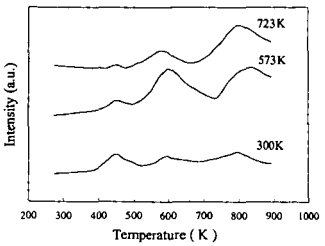

Figure 2. TPD profile over the used 8wt% nickel catalyst supported on alumina

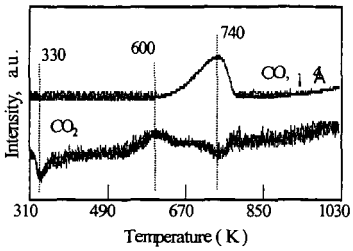

Figure 3. TPSR in CO_2/He (1:10) stream following CH_4 pulse at 973K over reduced Ni/Al_2O_3 catalyst.

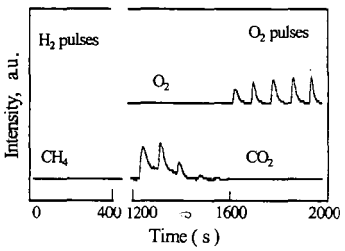

Figure 4. H_2 and O_2 pulses patterns at 973K following CO_2 TPSR over Ni/Al_2O_3 catalyst.

THE MICROWAVE PROMOTED CARBON CATALYZED PRODUCTION OF TERMINAL OLEFINS FROM LONG CHAIN ALKANES AND CARBON-CARBON CLEAVAGE REACTIONS OF ORGANIC MOLECULES

Dennis D. Tanner,[1] Qizhu Ding,[1] Pramod Kandanarachchi[2] and James A. Franz[2]

Contribution from the Department of Chemistry,
University of Alberta, Edmonton, Alberta, T6G 2G2, Canada
and
Pacific Northwest National Laboratory
Richland, WA 99352 USA

Key Words: Carbon-catalyzed, microwave, α-olefins, ethylene, hydrogen production.

ABSTRACT

The selective conversion of saturated linear hydrocarbons at ambient temperature to α-olefins and dihydrogen and other transformations of organic molecules involving the direct scission of carbon-carbon bonds are described. Activated wood charcoals containing trace metals were subjected to microwave radiation in the presence of liquid hydrocarbons at room temperature. Long-chain hydrocarbons were converted with high selectivity to a series of terminal olefins. For example, at less than 30% conversion, n-hexadecane yields n-C_3 to n-C_{14} α-olefins and light gases, predominately ethylene, and dihydrogen. Extensive conversion of linear hydrocarbons leads to substantial yields of α-olefins, diterminal diolefins, and ethylene. Product distributions are consistent with a pathway for olefin formation from linear hydrocarbons at room temperature that does not involve free radical formation. The method is effective for carbon-carbon bond cleavage in and conversion of a wide array of linear and branched hydrocarbon feedstocks to hydrogen, ethylene, and olefins. Saturated organic hydrocarbons containing functional groups (-OH, -CN, $-CO_2H$, $-CO_2CH_3$) undergo carbon-carbon bond scission and olefin formation with substantially intact functional groups. Cyclic alkanes and terpenoid hydrocarbons under ring cleavage, contraction, and ring isomerization reactions. In the presence of small amounts of water, cycloalkanes are converted to cyclic alcohols and ketones. The method makes possible selective chemical transformations involving the direct cleavage of saturated carbon-carbon bonds at room temperature.

INTRODUCTION

The direct cleavage of strong carbon-carbon bonds to effect selective synthesis of lower molecular weight hydrocarbons is a primary goal of research in heterogeneous and homogeneous catalysis. Methods for the selective, direct cleavage of strong carbon-carbon bonds, particularly at ambient temperature and atmospheric pressure, are scarce. Most approaches involve some degree of thermal hydrocracking to effect strong bond scission and structural isomerization, or the involvement of transition metal catalysts capable of activation of a hydrocarbon via oxidative addition of a hydrocarbon C-H bond to a coordinatively unsaturated metal system. Previous work with microwave-activated catalysis has involved creation of high local temperature regimes leading to thermal cracking and reforming involving free radicals, ions, carbenes, atoms and other reactive intermediates. Solution phase microwave promoted chemical transformations have generally dealt with either dielectric heating of the substrate or catalyst,[3] or with reactions carried out using a vapor phase plasma.[4] These approaches using dielectric heating involve the creation of "hot spots" in the catalyst surface that promote chemical transformations through local high temperature regimes.[5] Thus, thermolysis of methane over a glowing microwave catalyst produces ethylene, acetylene, propylene, hydrogen and soot reminiscent of simple thermal pyrolysis.[3d] Under more controlled conditions of low power irradiation, ethylene and acetylene may be prepared from methane and hydrogen with significant selectivity.[5] While previous studies have demonstrated that light organic gases can be converted under plasma initiation conditions, no previous work has explored the utility of microwave activated catalysis in bond-breaking transformations of large organic molecules and functionalized alkanes. Thus, in this work we present results of a study of low-power microwave irradiation of an activated carbon catalyst that leads to carbon-carbon bond cleavage and olefin formation from linear alkanes without formation of characteristic organic pyrolysis products. High yields of olefins and hydrogen result from a range of hydrocarbon precursors and functionalized hydrocarbons. Organic structures are demonstrated to exhibit significant chemical selectivity in carbon-carbon bond scission reactions, in part due to the ability of the liquid organic medium to rapidly quench high energy intermediates.

EXPERIMENTAL

Microwave Conversion of Hexadecane To Olefins. **Hexadecane** (2 g) was mixed with activated charcoal (0.5 g) in a reaction tube and subjected to microwave radiation (20 min) at 60% power

(ca. 30 watts) at 2540 MHz using the apparatus shown in Figure 2. The total volume of the gaseous products were measured by the gas burette, and both gaseous and liquid products were analyzed by GC, GC/IR and GC/MS. Products were identified by comparison of their GC retention times, GC/IR and GC/MS of authentic samples that were available. When the authentic samples were not available, products were identified by their GC/IR and GC/MS which showed similarities to those of authentic homologous compounds. Gaseous and liquid products are shown in Table 1.

Microwave Promoted Reaction of Polyethylene in the Presence of Wood Char. A sample of low density **polyethylene** (2 g) was heated to melt (>130°C) and mixed with activated charcoal (0.5 g) and subjected to microwave radiation for 2 minutes. The products were identified by means of GC, GC/IR and GC/MS and comparison with authentic materials. With extended irradiation, the molten polymer could be completed converted to volatile products consisting primarily of ethylene, along with hydrogen, and minor yields of light olefins and hydrocarbons.

Microwave Promoted Conversion of Diacid Esters. **Dimethyl-1,6-hexanedioic acid ester (Dimethyladipate)**. 0.1g of charcoal and 1 g of substrate were irradiated for 2 hours at 50W. The major products (30% conversion) were methyl acrylate, methyl butenoate, and methyl pentenoate, formed in the ratio 20:5:1. These products composed 85% of the product mixture. Minor products methyl proprionate, methyl butanoate, and methyl pentanoate were formed as 15% of the reaction mixture. Hydrogen was not quantitated in the reaction. These results suggest that dimethyl adipate was cleaved to form methylacrylate with 65% selectivity. **Dimethylmalonate**. 0.15g wood char and 2.5 g substrate were irradiated for two hours. This resulted in less than 4% conversion to gaseous products and less than ca. 1% conversion to liquid products (methanol and methyl acetate). **Diethylsuccinate**. 0.15 g wood char and 2.5 g substrate were irradiated for two hours. About 10% conversion to gaseous products (CO_2, CH_4, C_2H_2, C_2H_4) and 2% conversion to ethanol and ethylacrylate occurred.

Microwave Irradiation of Methyl Palmitate. **Methyl Palmitate** , 1 g and wood char, 0.1 g, were irradiated for 1 hour. Products included gases (C_2H_4, C_2H_2, H_2 and CO_2) accounting for 6% of starting ester and liquids accounting for 14% of the starting ester. The liquid products consisted of a series of terminal olefins, n-$C_3H_7CH{=}CH_2$ through n-$C_{13}H_{27}CH{=}CH_2$, along with a series of corresponding terminal olefins substituted with an ester group, $CH_3O_2C(CH_2)_nCH{=}CH_2$, n=4-12. The esters were each produced in yields comparable to its corresponding simple terminal olefin cleavage pair. This indicates that the ester group remained intact during the carbon-carbon scission reaction.

Microwave Irradiation of Octadecanol. **1-Octadecanol**, 1 g, and pine char, 0.05 g, were irradiated at ca. 50 W for one hour. At ca. 30% conversion, products consist of light gases (ca. 50%), the major component of which is ethylene, and liquids (ca. 50%). The liquid products were composed of a series of terminal olefins and a corresponding series of terminal olefins possessing a terminal hydroxyl group ($C_3 - C_{17}$). The hydroxylated hydrocarbon terminal olefins and hydrocarbon terminal olefins were formed in approximately equal yields.

Microwave Irradiation of Cyclododecane. **Cyclododecane** (damp with water, or dried, by exposure of a solution of hydrocarbon in CH_2Cl_2 to anhydrous $MgSO_4$), 1 g, and white pine char catalyst, 0.05-0.1 g, were warmed to ca. 100 °C to melt the waxy hydrocarbon after which irradiation (ca. 50 W) was carried out for 20 min. Dry cyclododecane underwent ca. 21% conversion in 10 min, yielding gaseous products (11%) and liquid products (10%). The liquid products include ring contraction products (22%), acyclic terminal olefins (56%), and acyclic diterminal olefins (14%). The gaseous products contained hydrogen (16%), methane(4%), ethylene (48%), ethane(2%), acetylene (12%), propylene(8%), butene(3%) and butadiene(7%). Damp cyclododecane gave cyclododecanol (19%) and cyclododecanone (26%) as major products, in addition to hydrocarbon products. In the absence of moisture, the products were as follows: C_{12} Products: 1-dodecene (14%); C_{10} Products: Cyclodecane (21%), 1-methyl-2-propylcyclohexane (2%), n-butylcyclohexane (4%), 1-decene (10%) and 1,9- decadiene(1%); C_9 Products: 1-nonene (4.6%), 1,8-nonadiene; C_8 Products: Cyclooctane (19.5%), 1-octene(7.5%), 1,7-octadiene (2%); C_7 Products: 1-heptene(3%), 1,6-heptadiene (1.6%); C_6 Products, cyclohexane (2%).

RESULTS AND DISCUSSION

Ambient Temperature Conversion of Linear Hydrocarbons. Low power microwave irradiation of liquid hydrocarbons in the presence of a catalyst, activated wood charcoal, leads to the remarkably selective production of α-olefins. In the case of hexadecane, conversion up to ca. 30% leads only to α-olefins and light gases, mainly ethylene. Above 30% conversion, the formation of diterminal diolefins becomes significant, and further conversion of lighter olefins to ethylene occurs. Ultimately, ethylene is the major product from hydrocarbons, with small yields of acetylene from further conversion of ethylene and butadiene. The terminally unsaturated hydrocarbons, C_3-C_{13}, formed from hexadecane are shown in Fig. 1 and Table 1. The gaseous products gave a 47% yield while the liquid products showed a 10% yield, see Table 1. The most notable features of the reaction include (1) the formation of α-olefins from linear alkanes with only trace levels of hydrocarbons, (2) the absence of internal (non-terminal) olefins, and (3) the

absence of alkyl radical termination products (saturated alkanes of higher molecular weight than the parent hydrocarbon). GC analysis of the products of hexadecane reaction and those of other linear hydrocarbons gave no more than trace quantities of simple hydrocarbons and no detectable longer chain ($> C_{16}$) hydrocarbons. Linear alkanes would have been formed in radical-radical termination reactions. Shorter chain fully saturated hydrocarbons would have been formed in radical-radical termination reactions and in abstraction reactions. Finally, some internal (non-terminal) olefins should have formed from disproportionation of secondary alkyl radicals formed in a radical forming initiating process. The absence of these products rules out the buildup of appreciable concentrations of free alkyl radicals as might be expected in a simple pyrolytic free radical mediated bond scission mechanism, at least in the nominally ambient temperature reactions.

Conversion of Polyethylene and More Complex Organic Structures. At the higher temperatures used to melt polyethylene (180 °C), saturated hydrocarbons were formed as minor products in addition to the major products, α-olefins, see Fig. 3. The production of alkanes is consistent with participation of the *functional equivalent* of diradicals or radical pairs resulting in disproportionation leading to the observation of alkane formation.

Conversion of Diesters. Dimethyl adipate, **1**, was found to react much faster than diethylsuccinate, **2**, and dimethyl malonate, **3**, which was nearly inert to the reaction conditions. Dimethyl adipate reacted with about 65% selectivity to give central carbon-carbon bond cleavage yielding methyl acrylate. These observations suggest that surprisingly selective transformations involving cleavage of strong carbon-carbon bonds are made possible by microwave activated catalysis.

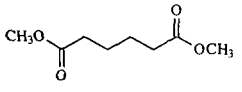

1

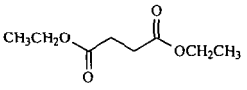

2

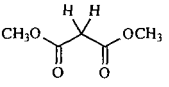

3

Conversion of Cyclic Hydrocarbons. The reaction of cyclododecane, carried out at 100°C, led to ring contraction products cyclodecane and cyclooctane in high yields at short reaction time. This implies that both products are first-generation products, and suggests a path for sequential loss of ethylene units, via the functional equivalent of a diradical pathway, as indicated in Figure 5. This would further seem to suggest that linear alkanes would form alkyl radicals by simple followed by multiple ethylene scission events and a terminating hydrogen atom elimination:

$$CH_3(CH_2CH_2)_x\bullet \rightarrow CH_3(CH_2CH_2)_{x-n}\bullet + n\,C_2H_4 \rightarrow CH_3(CH_2CH_2)_{x-n-1}CH{=}CH_2 + H\bullet$$

Such a scheme would be consistent with the substantial yields of ethylene at low overall conversion of linear hydrocarbons, but it would appear inconsistent with the absence of alkyl free radical products, e.g., the absence of alkane products from abstraction, combination, and disproportionation.

The microwave irradiation of a char catalyst at low power levels is accompanied by the emission of flashes of light. A number of reaction pathways can be proposed for fragmentation of alkanes in the local high temperature plasma regime generated in such a catalyst discharge zone. Among a variety of possibilities, the creation of a coordinatively unsaturated metal site can be envisioned to undergo oxidative insertion into alkanes leading to olefin and dihydrogen formation, see Figure 4.

Catalyst Lifetime. Wood char catalysts exhibited long lifetimes under the conditions of liquid phase hydrocarbon conversion. The wood char catalysts could be used repeatedly by recharging the reactor cell (Fig. 2) with hydrocarbon substrate. The catalyst could be irradiated at low power (ca. 50 W) with no drop in activity after up to eight hours. Thus, the method is suitable for continuous conversion of hydrocarbons and other substrates to olefins and hydrogen.

Summary. The direct cleavage of strong carbon-carbon bonds, leads to a wide variety of potential natural product, biomass, carbohydrate, cyclic and acyclic hydrocarbon bond cleavage reactions, many of which can be envisioned to occur with sufficient chemical selectivity to be of synthetic use. In addition, the present results indicate the potential for use of microwave activated catalysis for the oxidation of hydrocarbons to ketones and alcohols.

ACKNOWLEDGEMENT

JAF and PK acknowledge the support by the Office of Energy Research, Office of Basic Energy Sciences, U.S. Department of Energy, under contract DE AC06 1830 RLO.

REFERENCES

1. Department of Chemistry, University of Alberta, Edmonton, Alberta.
2. Pacific Northwest National Laboratory, Richland, WA.
3. (a) Dayani, R. "Molecular Magic With Microwaves," *Chem. Eng. News*, **1997**, Feb. 10th, *26*.
   (b) von Hippel, A.R. "Dielectric Materials and Applications," MIT Press, Cambridge, MA., USA **1954**.
   (c) Gabriel, C.; Gabriel, S.; Grant, E.H.; Halstead, B.S.J.; Mingos, D.M.P. Dielectric Parameters Relevant to Microwave Dielectric Heating," *Chemical Society Reviews*, **1998**, *27*, 213.
   (d) Majetich, G.; Wheless, K. "Microwave-Enhanced Chemistry," *American Chemical Soc. Publication*, H.M. Kingston and S.J. Haswell, Eds. **1997**, Chapter 8.
4. (a) Beeri, A.; Berman, E.; Vishkautsan, R.; Mazur, Y. *J. Am. Chem. Soc.*, **1986**, *108*, 6413.
   (b) Tanner, D.D.; Zhang, L. *J. Am. Chem. Soc.*, **1994**, *116*, 6683.
   (c) Tanner, D.D.; Kandanarachchi, P.; Das, N.C.; Brausen, M.; Vo, C.T.; Camaioni, D.M.; Franz, J.A. *J. Org. Chem.*, **1998**, *63*, 4587.
   (d) Tanner, D.D.; Zhang, L.; Kandanarachchi, P. *J. Phys. Chem.*, **1996**, *100*, 11319.
5. Mingos, D.M.P.; Whittaker, A.G. *J. Chem. Soc., Dalton Trans.*, **1992**, 2751.
6. For examples of Microwave activated catalysis, see
   (a) A. Revella; Murphy, W.J.; Achia, Biddanda V. "Conversion of C_2+ Hydrocarbons Using Microwave Irradiation", U.S. Pat. 4,975,164 (1990).
   (b) J.K.S. Wan, "Microwave Induced Catalytic Conversion of Methane to Ethylene and Hydrogen",U.S. Pat. 4,574,038 (1986).
   (c) J.K.S. Wan, U.S."Microwave Production of C_2 Hydrocarbons Using a Carbon Catalyst", Pat. 5,472,581 (1995).
   (d) W.J. Murphy, "Conversion of Methane Using Pulsed Microwave Radiation",U.S. Pat. 5,205,912 (1993).
   (e) W.J. Murphy, "Conversion of Hydrocarbons Using Microwave Radiation", U.S. Pat. 5,277,773 (1994).
   (f) W.J. Murphy, D.H. Shaw, "Upgrading of Low Value Hydrocarbons Using A Hydrogen Donor and Microwave Radiation"" U.S. Pat 5,181,998 (1993) and U.S. Pat. 5,328,577 (1994).

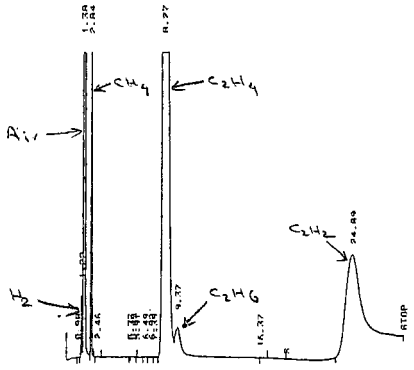

Figure 1a. GLPC Chromatogram of Gaseous Products from the Microwave Irradiation of Hexadecane in the Presence of Wood Char.

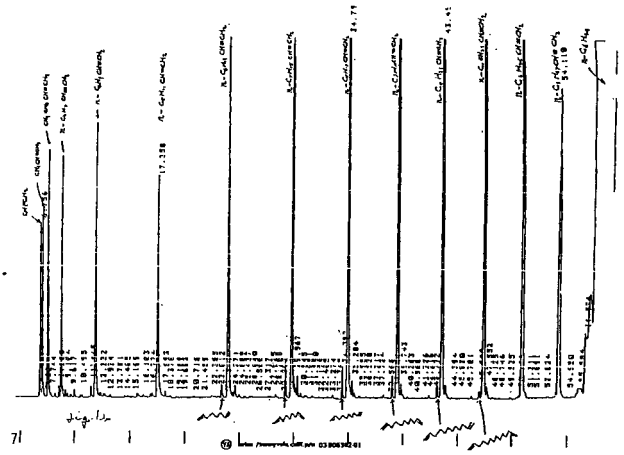

Figure 1b. Glpc Chromatogram of Liquid Products from the Microwave Irradiation of Hexadecane in the Presence of Wood Char.

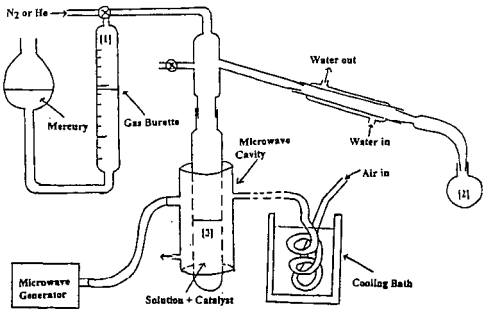

Figure 2. Apparatus for the Microwave Irradiation of Hydrocarbons.

Product	% Yield (Mole basis)
Liquid Products[a], 100-minute reaction	
n-$C_3H_7CH=CH_2$	0.59
n-$C_4H_9CH=CH_2$	1.22
n-$C_5H_{11}CH=CH_2$	1.24
n-$C_6H_{13}CH=CH_2$	3.23
n-$C_7H_{15}CH=CH_2$	14.7
n-$C_8H_{17}CH=CH_2$	17.6
n-$C_9H_{19}CH=CH_2$	14.8
n-$C_{10}H_{21}CH=CH_2$	13.4
n-$C_{11}H_{23}CH=CH_2$	13.2
n-$C_{12}H_{25}CH=CH_2$	13.6
n-$C_{13}H_{27}CH=CH_2$	6.27
Gaseous Products[b]	
H_2	12.0
CH_4	4.83
C_2H_4	40.9
C_2H_6	2.05
C_2H_2	7.12
C_3H_8	16.5
$CH_3CH_2CH=CH_2$	8.16
$CH_2=CHCH=CH_2$	5.79
Others	2.17

[a]Products normalized to 100%. [b]Products normalized to 100%

Table 1. Products from Microwave Irradiation of Hexadecane in the Presence of Wood Char.

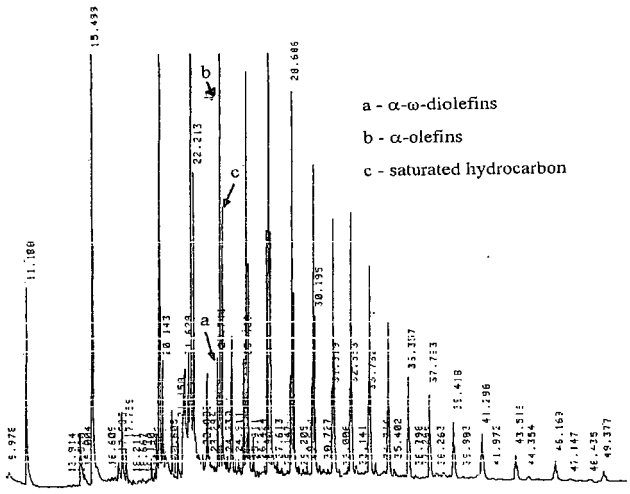

Figure 3. Products Formed from the Catalytic Microwave Oxidative Fragmentation of Polyethylene.

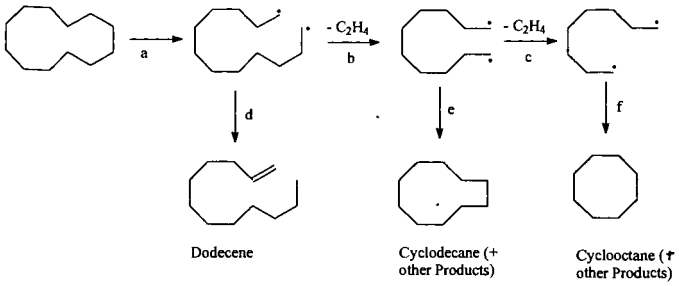

Figure 4. Biradical Mechanism for Hydrocarbon Conversion. Biradical Formation (a) followed by sequential ethylene loss (b,c) with product formation by disproportionation (d) or ring closure (e,f).

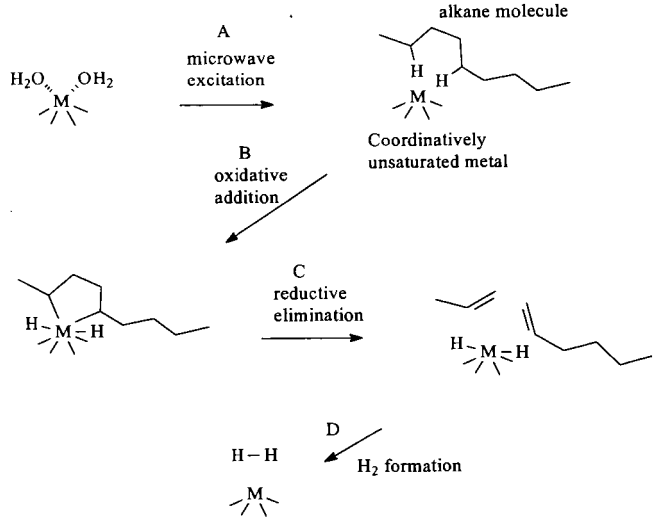

Figure 5. Metal-Centered Catalysis Mechanism for Oxidative Fragmentation of Alkanes.

ENERGY AND EXERGY ANALYSIS OF FCC UNIT

Chun-Min Song, Yong-Shan Tu, Zi-Feng Yan*
State Key Laboratory for Heavy Oil Processing, University of Petroleum, Dongying, 257062, P R CHINA

ABSTRACT The energy and exergy balances were effectively calculated by the three-section model and the two-box method on the basis of field data of the FCC unit. The results show that the net energy consumption of the FCC unit is 2197.60MJ/t. Simultaneously, the efficiency of the exergy of the conversion section is rather poor, and the energy losses of the recovery section are much higher. The losses of the energy and exergy of regenerator are greatest in the conversion section. It means that it is not enough only to reduce the heat losses of the flue gas, the exergy losses of the process is also important to the reduction of the coke formation. In conclusion, the calculations show that conversion and recovery sections have more potential to the reduction of energy consumption. It indicated that the key factors are to reduce the energy consumption of the regenerator, optimize the heat exchanging system and utilize the low temperature heat.

KEYWORDS: catalytic cracking; energy consumption; exergy analysis

1. INTRODUCTION

Catalytic cracking is one of the most important petroleum refining processes. The most significant characteristic of the cracking process is its flexibility in treating the variety of feedstock available from the crude currently being refined, which becomes increasingly important, as refiners are obliged to resort to heavier crude containing refractory or poisonous constituents, due to shortages and to the high price of the more desirable crude. Many technologies are applied to the FCC processes for raising the operating efficiency, innovated decreasing the energy consumption, producing high quality products, and obtaining more remarkable economic benefits. However, the flexibility of the FCC process is negatively weakened by the excessive energy consumption. Thus, the improvement of the efficiency of the energy utilization has been the subject of investigations designed to optimize the fundamental problems in engineering and processes. The great majority of such investigations has been conducted by petroleum companies and held confidential in order to improve the economic benefits. It suggested that the majority of the energy and exergy analysis is purely "applied". Because of the highly "applied" nature of this work in the field, understanding of the various phenomena involved in FCC process is far from complete. In order to understand the effect of energy consumption in FCC process, two kinds of analysis methods of energy and exergy are usually employed in the cracking process.

(1) three-section model[1]. The conversion and transport of energy, technology utilization and energy recovery, i.e., three-sectionm odel of energy analysis is adopted according to the clue of energy utilization and evolution.

(2) two-box method[2]. The gray-box and black-box methods are applied to energy analysis in terms of different systems and equipment involved. The degree of energy utilization of the systems and equipment is available by this method.

The paper aims to study the energy utilization level of the catalytic cracking process employing three-section model and gray-box or black-box methods.

2. EXPERIMENTAL

All field data used in this paper were collected with locale unit. On the basis of field data of the FCC unit, the energy and exergy balances were calculated by the three-section model and the two-box method.

3. ENERGY AND EXERGY BALANCE ANALYSIS

The overall evaluation of the energy consumption according to three-section model is shown in table 1. The net energy consumption and primary energy consumption of the FCC unit amount

* To whom correspondence should be addressed. Email: zfyan@hdpu.edu.cn

to 2197.60 and 2425.43MJ/t, respectively. The conversion and recovery section suffer from high-energy loss and has much potential to improve. The energy and exergy balance analysis is conducted employing gray-box method according to three-section model and the evaluation results of the three-section are shown in table 2[3].

The energy conversion section consists of regenerator (included flue gas energy recovery system), main air blower, gas compressor and pumps. The regenerator suffers great energy and exergy losses with the respective loss coefficient of 21.0% and 41.7%. The energy and exergy analysis of the regenerator is calculated according to the gray-box model and results are shown in table 3. The utilization efficiency and losses of the energy and exergy are evaluated.

The heat exchanger and condenser are made up of the energy recovery section. The cooling energy and exergy are abandoned and puts on the loss item, so only the total cooling energy and exergy are calculated. A portion of energy and exergy of the heat exchanger are lost in the recovery section. The energy and exergy analysis of the heat exchanger is carried out employing black-box model and the results are shown in table 4.

4. DISCUSSION

4.1 Conversion section

It can be seen from table 2 and 3 that the regenerator and recovery system suffer the greatest energy and exergy losses and supply a low energy utilization efficiency of 77.18.The recovery heat energy of the flue gas should be paid attention due to the high energy losses coefficient of 16.80 . Simultaneously the results of the exergy analysis show that the process exergy loss coefficient of 35.16 is much higher than the exhausting flue gas exergy loss coefficient of 6.11 . It means that it is not enough only to reduce the heat losses of the flue gas, the reduction of the exergy losses of the process is more important. The process exergy losses, which consists of the irreversible burning loss of the coke and the heat transfer loss, becomes the weak section of the energy utilization and also the potential aspect to the reduction of energy consumption of the conversion section. The key to reduction of the exergy losses of the regenerative process lies in suppressing coke yield so as to decrease exergy loss of the burning process.

The pressure and heat energy of the flue gas should be recovered in order to improve energy utilization efficiency of the regenerator. The pressure energy of the flue gas can be recovered by the flue gas expander, while the utilization degree of the sensible heat of the flue gas depend on its exhaust temperature. The flue gas expander generated horsepower directly going into the electrical network. In this unit the recovery power ratio (the power ratio of flue gas expander to the air blower) of 73% is lower. The design capacity of the flue gas expander is smaller to partial bypass of flue gas and the heat loss of the flue gas pipelines is greater. Therefore the recovery power ratio can be increased to 114% if pressure energy of flue gas is sufficiently utilized. The expander has a horsepower recovery potential exceeding the requirements of the air blower. In this way, the work recovered by the flue gas expander not only maintains the regular operation of the air blower, but also generate a part of electricity.

The waste heat boiler is used to produce the middle pressure steam of 3.6MPa, and the exhaust temperature of flue gas is at 256, of which energy can be farther recovered. Furthermore, only 65% flue gas flows into the waste heat boiler. It means that 35% of flue gas is exhausted with high temperature of 526. In a word, it is necessary to reduce the direct emission and recover the heat of flue gas more efficiently.

The efficiency of pumps is generally low, 71% of pumps operated with the efficiency below 50%. It indicates that it is worthy to improve the efficiency of the pumps. The application of new type high-efficiency pump or electric machine with frequency converter may be a good choice to improve the drive conversion efficiency. By so doing, electricity energy can be saved.

Although, the power losses of conversion process was lower, but the value high to the other formal energy, hence it cannot be ignored.

4.2 Technology utility section

The total supplied energy of the technology utility section is 2740.76MJ/t, has higher level. Of special is that the proportion of the recovery cycle energy and exergy is low, with 22.5 and 12.7 of the total supplied energy, respectively.

The thermodynamic energy and exergy consumption is that the total supplied energy and exergy transform to the part of the products , with the respective ratio of 19.0 and 27.4. It indicates that the decline of the total supplied energy is also a potential route to improve the energy and exergy consumption.

In technology utility section, exergy losses coefficient of heat dissipated is 3.64 , exergy losses of the process is 18.54 . It means that the reaction and fractionation processes contribute very much to the exergy losses.

The energy utility level of the main fractionation tower has quite influence on the total energy consumption. The exergy loss of the fractionation tower is mostly derived of heat transfer. Therefore heat removal by the top reflux should be minimized while more heat can be removed by hot mid-section reflux and slurry oil reflux if the product quality and yields are ensured. Additionally it is a method to minimize the temperature difference between inlet and outlet tower flows of the reflux.

4.3 Energy recovery section

The ratio of energy and exergy recovery were 54.43 and 45.97, respectively. The cooling energy and exergy losses were 38.39 and 29.56 accordingly in the section supplied energy.

The cooling losses of the whole unit constitutes 35.6 of the net energy consumption and becomes the chief part of the energy consumption. The crux of reducing the cooling(heat rejection) loss rests with the utilization of low temperature heat owing to the most heat below

120 .

The data in table 4 indicate exergy losses coefficient of the heat exchanger network reaches 27.69%. The high temperature difference of heat transfer brings about the great exergy losses. The exergy losses of heat transfer can be inhibited by the optimization of the heat exchanger system.

5. APPROACH OF ENERGY SAVING

The energy conversion and recovery become the weak section of the energy utilization. But technology utility section is core of energy utility. It determines the amount of energy available from recovery and conversion sections. As a result, to minimize the total supplied energy of the technology utility section is the first consideration, subsequently the recovery and conversion sections are considered.

(1) Reducing total supplied energy of the utility section

Introducing advanced technology, optimum catalysts and effective additives are front problems to reducing the total supplied energy of the technology utility section. Besides little heat of steam is utilized in the technology section. The introduction of advanced technical measurements may be a choice to decrease the amount of steam used. For example the dry-gas prelifting technology can not only save energy but also cut down dry gas and coke yield. In addition, appropriate low temperature heat may be used to supply instead of the accompanying steam.

The throttle losses of the exit valve can be reduced through the selection of proper pumps. For the pump with frequent flux change, the variable-frequency electric machine is a good substitute for elevation of pump efficiency and decline of electrical energy.

(2) The optimization of heat exchanger network is an effective way to decrease heat transfer exergy losses and improving the energy recovery ratio. In the first step, the heat exchangers with the temperature difference upwards of 30 s hould be eliminated. Secondly, it is worth while to enhance the heat preservation of high-temperature position. Finally, the integrated utilization of low-temperature heat becomes more and more important with the deepening of the idea of energy savings. A great deal of low-temperature heat supplied with catalytic cracking process can be made use of heating medium of other units or devices, such as preheating water supply and living heating in winter, etc. Next low temperature heat may be considered to upgrading utility, which might face the lower efficiency and higher investment.

(3) The energy utilization efficiency of the regenerator lies on the recovery and utilization of flue gas due to the adoption of the complete combustion technique. Hereby, it is important for the regenerator and energy recovery system to maintain the flue gas expander operates in a perfect performance. In addition, the heat of flue gas should be recovered sufficiently by the waste heat boiler. In a word, it is very significant for the energy saving to maintain the long-cycle, full-loaded, and high-efficient running of the flue gas expander and the waste heat boiler.

6. CONCLUSIONS

The measures of energy saving must be determined in the opinion of energy and exergy balance analysis. For the catalytic cracking unit with the flue gas expander and waste heat boiler, the recommended measurements of energy saving are as follows:

(1) Improving the recovery and utility ratio of the flue gas expander and reducing exhausting temperature of the waste heat boiler. Maintaining the long-cycle, full-loaded, and high-efficient running of the flue gas expander and the waste heat boiler.

(2) Optimizing the heat-exchanging network to reduce temperature difference of heat transfer of the heat exchangers.

(3) Strengthening the integrated utilization of low temperature heat.

ACKNOWLEDGMENTS

We would like to express our gratitude to Rong-Gang Ding for his contributions to write the article.

REFERENCES

[1] Ben Hua. Energy utility analysis and integration of technology processes. Hydrocarbon Processing Press, 1989.p2522 8 8.

[2] Xinyue Xiang. Engineering exergy analysis method. Petroleum Industry Press, 1990.

[3] Anmin Chen. Energy saving method and technique of petrochemical processing. China Petrochemical Press, 1995.

Table 1 the recapitulation statement of energy and exergy analysis using of three-section model

Item		Energy	Exergy
Net energy(exergy) consumption MJ/t		2197.60	2221.96
Primary energy consumption MJ/t		2425.43	
Total supplied energy (exergy) of utilization section MJ/t		2740.76	1455.72
Conversion efficiency		78.30	56.57
Energy utilization efficiency		93.32	77.82
Recovery rate		54.43	45.97
Total ejected energy and exergy MJ/t		1639.57	531.93
Total process exergy losses MJ/t			1255.71
Losses MJ/t :			
	Conversion section	534.42	1067.11
	Utilization section	182.94	322.84
	Recovery section	927.70	396.59

Table 2 The recapitulation statement of gray-box of "three-section" model

Item			energy analysis		exergy analysis	
			Energy MJ/t	Energy loss coefficient %	Exergy MJ/t	Energy loss coefficient %
Energy conversion section	Input	Regenerator	2342.06		2245.29	
		Main air blower	139.42		139.42	
		Gas compressor	42.00		50.42	
		Pump	21.98		21.98	
		Sum	2545.46		2457.11	
	Output	Regenerator	1807.64		1220.02	
		Main air blower	135.39		125.69	
		Gas compressor	39.20		33.38	
		Pump	10.91		10.91	
		Sum	1993.14		1390.00	
	Losses	Regenerator	534.42	21.00	1025.27	41.73
		Main air blower	4.03	0.16	13.73	0.56
		Gas compressor	2.80	0.11	17.04	0.69
		Pump	11.07	0.43	11.07	0.45
		Sum	552.32	21.70	1067.11	43.43
Utilization section	Supplied energy		2740.76		1455.72	
	Thermodynamic energy and exergy consumption		522.09		398.93	
	Exergy Losses	Reactor			135.08	9.28
		Main fractionator			91.42	6.28
		Other units			43.39	2.98
		Sum			269.89	18.54
	Losses of rejection of heat		182.94	6.67	52.95	3.64
	Needed recovery energy		2035.72		733.96	
Recovery section	Recovery cycle		616.63		184.66	
	Recovery output		491.39		152.71	
	Losses	Heat losses	63.77	3.13	19.39	2.64
		Cooling	781.51	38.39	216.96	29.56
		Other	82.42	4.05	5.75	0.78
		Sum	927.70	45.57	242.10	32.98

Exergy losses	Condenser and heat exchanger	124.18	16.92
	Other	30.31	4.13
	Sum	154.49	21.05

Table 3 The results of the regenerator and energy recovery system

Item	Energy MJ/t	Energy loss coefficient	Exergy MJ/t	Exergy loss coefficient
Supplied energy(exergy)	2342.06		2245.29	
Useful energy(exergy)	1807.64		1220.02	
Energy utilization efficiency	77.18			
Exergy utilization efficiency			54.34	
Exhaust flue gas	393.44	16.80	137.22	6.11
CO chemical energy	8.90	0.38	8.90	0.40
Heat losses	127.04	5.42	88.36	3.93
Other	5.04	0.22	1.44	0.06
Process exergy losses			789.35	35.16
Total	534.42	22.82	1025.27	45.66

Table 4 The black-box analysis results of heat exchanger

Energy analysis			Exergy analysis		
Item	Energy MJ/t	Energy loss coefficient	Item	Exergy MJ/t	Exergy loss coefficient
Supplied energy	871.77		Supplied exergy	381.60	
Recovery energy	840.15		Recovery exergy	265.38	
Heat losses	31.62	3.63	Exergy losses of heat	10.55	2.76
			Process exergy losses	105.67	27.69
Total energy losses	31.62	3.63	Total exergy losses	116.22	30.45